Eur. Phys. J. C 4, 249–257 (1998)
DOI 10.1007/s100529800804

THE EUROPEAN PHYSICAL JOURNAL C

Neutral meson production in p-Be and p-Au collisions at 450 GeV beam energy

G. Agakichiev[1a], M. Appenheimer[2], R. Averbeck[3], F. Ballester[4], R. Baur[5], A. Brenschede[2], J. Diaz[4], A. Drees[5], U. Faschingbauer[1], J.L. Ferrero[4], P. Fischer[5], Z. Fraenkel[6], M. Franke[2 b], Ch. Fuchs[1], E. Gatti[7], P. Glässel[5], Th. Günzel[5], C. P. de los Heros[6], F. Hess[1], R. Holzmann[3], D. Irmscher[5], C. Jacob[1], W. Kühn[2], B. Lenkeit[5], H. Löhner[8], A. Marin[4], F.M. Marques[4], G. Martinez[4], V. Metag[2], M. Notheisen[2,b], R. Novotny[2], L. H. Olsen[5], R. Ostendorf[9], Y. Panebrattsev[1,a], A. Pfeiffer[5], I. Ravinovich[6], P. Rehak[10], M. Sampietro[7], A. Schön[5], J. Schukraft[11], Y. Schutz[9], S. Shimansky[11,a], A. Shor[6], R.S. Simon[3], H. J. Specht[5], V. Steiner[6], S. Tapprogge[5], G. Tel-Zur[6], I. Tserruya[6], Th. Ullrich[5], H. Wilschut[8], J. P. Wurm[1], and V. Yurevich[7,a]

[1] Max-Planck-Institut für Kernphysik, D-69117 Heidelberg, Germany
[2] II. Physikalisches Institut der Universität Gießen, D-35392 Gießen, Germany
[3] GSI, D-64220 Darmstadt, Germany
[4] Instituto Fisica Corpuscular, E-46100 Burjassot Valencia, Spain
[5] Physikalisches Institut der Universität Heidelberg, D-69120 Heidelberg, Germany
[6] Weizmann Institute, Rehovot 76100, Israel
[7] Politecnico di Milano, I-20133 Milano, Italy
[8] Kernphysisch Versneller Institut, NL-9747AA Groningen, Netherlands
[9] GANIL, F-14021 Caen, France
[10] Brookhaven National Laboratory, Upton, NY 11973, USA
[11] CERN, CH-1211 Geneva 23, Switzerland

Received: 2 July 1997 / Published online: 5 June 1998

Abstract. In a joint experiment the TAPS and CERES collaborations have studied the production of the neutral mesons π°, η and ω in 450 GeV p-Be and p-Au collisions at the CERN SPS. The mesons were identified by their $\pi^\circ \to \gamma\gamma$, $\eta \to \gamma\gamma$, and $\omega \to \pi^\circ\gamma$ decay modes. The cross sections were measured down to very low p_T (≥ 20 MeV/c) near mid-rapidity ($3.0 < y < 4.0$). The η and ω cross sections are smaller than expected from extrapolations of earlier data to low p_T. Integrated over all p_T, the ratios η/π° and ω/π° are lower by about 25% compared to previously published values. The reduction may be attributed to the large number of low p_T pions from decays of heavier mesons. In addition, we have studied the dependence of neutral meson production on the mass of the nuclear target and find it in good agreement with previous measurements of charged mesons.

1 Introduction

Meson production in high energy hadron collisions has been studied over the last 30 years. Detailed results are available on pion production but data on heavier mesons like η and ω are scarce, in particular at low transverse momenta p_T. The interest in meson production at low p_T is twofold:

On the one hand, these data provide a test of our understanding of the dynamics of soft hadron collisions. The observations have mostly been interpreted in terms of phenomenological descriptions since a rigorous treatment within the framework of non-perturbative QCD is not yet possible. The most successful phenomenological description – published by M. Bourquin and J.M. Gaillard in 1976 [1] – parameterizes the double differential cross section $d^2\sigma/dp_T dy$ for all particles in a large $\sqrt{s}$ region from 6 to 63 GeV. Different particle species are only distinguished by their transverse mass $m_T = \sqrt{m^2 + p_T^2}$. Over the past 20 years the BG-parameterization has withstood a large amount of new data. However, up to today, the p_T range below 300 MeV/c has mostly been studied using pion data.

On the other hand, the cross sections for neutral mesons have to be known with high precision in order to determine the contribution of π°, η, and ω decays to low mass lepton pair production. This is extremely important to properly address the long-standing problem of the so-called anomalous excess of low-mass pair production (m = 200 - 600 MeV/c^2) that was claimed by several groups [2] over the last two decades and that dramatically decreased with improved measurements of the HELIOS

[a] visiting from JINR, Dubna, Russia
[b] Doctoral Thesis of M. Franke and M. Notheisen, Universität Gießen (1996)

collaboration. In a recent paper HELIOS quotes an upper limit of ∼40% [3] on additional sources of lepton pairs not accounted for by either direct or Dalitz decays of neutral mesons.

In a joint effort the CERES and TAPS collaborations have performed a coincidence measurement of e^+e^--pairs and photons in 450 GeV p-induced collisions [4]. The main goal was to further increase the sensitivity to new sources of dileptons. As in the experiment of HELIOS-1, photons and lepton pairs were detected in coincidence to allow a direct measurement of the Dalitz decay contributions to inclusive lepton pair production. In an effective beam time of 30 days, e^+e^- and $e^+e^-\gamma$ data were recorded for p-Be and p-Au. The results of this measurement are published separately [5]. Simultaneously, the experimental setup provided the opportunity to measure the production of neutral mesons via their photon decay modes. For this purpose a small fraction of the beam time was dedicated to a high statistics photon measurement using only the electromagnetic calorimeter TAPS.

This paper is restricted to the results of the dedicated photon measurement. It is structured as follows: Sects. 2, 3, and 4 describe the experimental setup, the data analysis and the determination of detector efficiencies. The results are presented in chapter 5. They are discussed and compared to previous measurements in chapter 6.

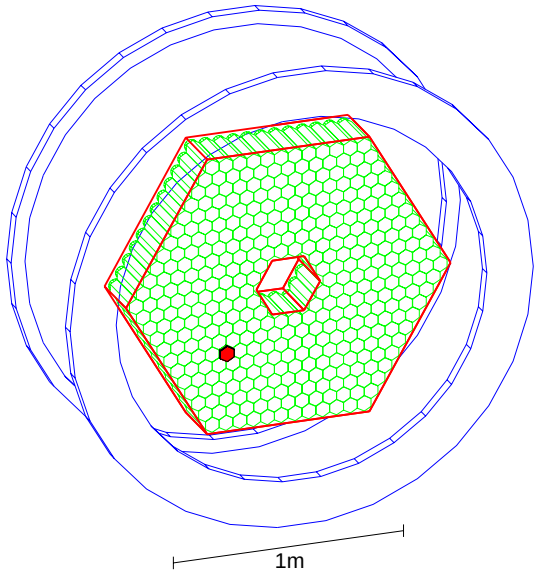

Fig. 1. Setup of the TAPS photon spectrometer at the CERN SPS. The 378 BaF_2 detectors are mounted in a wall 6 m downstream from the target. The magnetic coils serve to compensate the magnetic field of the CERES spectrometer. A charged particle veto detector shown in black is mounted in front of one of the BaF_2 modules

2 Calorimeter setup

The electromagnetic calorimeter TAPS [6] was positioned downstream of the CERES spectrometer [7]. The calorimeter comprised 378 hexagonally shaped BaF_2 crystals with a depth of 12 radiation lengths and a width of 59 mm. The detectors were arranged in a hexagon around the beam axis (shown in Fig. 1) to realize a full azimuthal coverage. It was located 6 m downstream of the target, covering the pseudorapidity range $3.0 < \eta < 4.0$ approximately centered around mid rapidity ($\eta = 3.4$ for pp-collisions at 450 GeV beam energy). In order to study the photon/hadron separation one crystal was equipped with a charged particle veto detector.

For data taking, we used a minimum bias interaction trigger. The trigger required a charged particle multiplicity $N_{ch} \geq 2$, measured with a silicon pad detector that was located 10 cm downstream of the target covering a pseudorapidity range from 2.0 to 3.0 [8].

3 Reconstruction of photons and neutral mesons

3.1 Shower reconstruction

Electromagnetic showers are reconstructed by searching for localized energy depositions in the calorimeter. A group of crystals with one local maximum (central crystal) above a certain threshold is regarded as a single shower candidate. Candidates are only accepted if the central crystal is within the fiducial area which excludes crystals on the inner and outer border of the hexagon. Consequently, a complete reconstruction of the showers is guaranteed. Signals not originating from the target are suppressed by applying a time-of-flight cut for each BaF_2-crystal. Signals from minimum ionizing particles are removed by an energy cut of 300 MeV on the central crystal. The total energy of a shower is determined by adding the energies of the 6 neighboring crystals to the value of the central crystal. The shower position is calculated as the center of gravity of the energies. Because of the relatively coarse granularity of the detector compared to the lateral shower dimension, a correction of the reconstructed shower position has been applied, resulting in a position resolution of $\sigma \sim 5$ mm.

3.2 Photon and hadron separation

The distinction between hadronic and electromagnetic showers is based on the different lateral development of hadronic and electromagnetic showers, which is reflected in the width and fluctuation of the shower. A frequently used measure is the second central moment of the lateral energy distribution, i.e. the shower dispersion:

$$D_x^2 = \frac{\sum A_i x_i^2}{\sum A_i} - \left(\frac{\sum A_i x_i}{\sum A_i}\right)^2 = \bar{x^2} - \bar{x}^2 \qquad (1)$$

and correspondingly for the other coordinates, where A_i is the pulse height and x_i the position of the ith module. Figure 2 shows the results of the lateral dispersion analysis of photons and hadrons, deduced from data of the

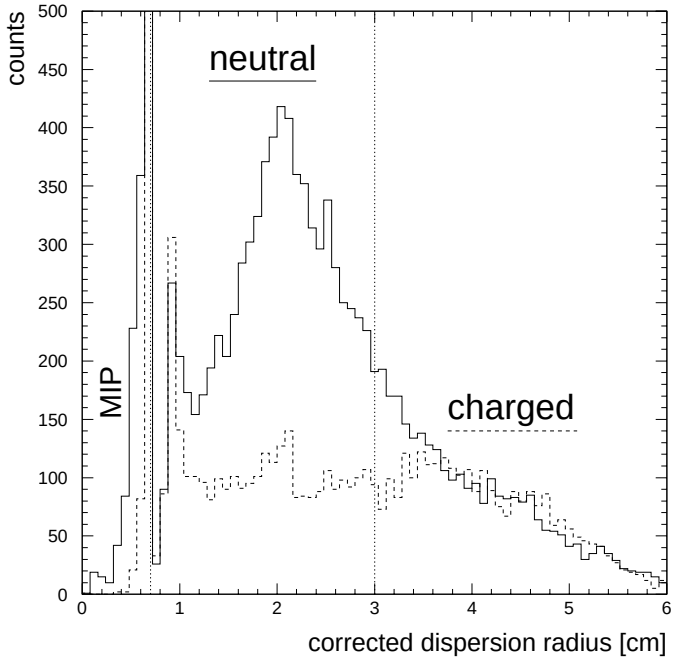

Fig. 2. Lateral dispersion of the energy deposited by photons and charged hadrons in the calorimeter. Photons and charged particles were distinguished by the veto detector in front of one crystal. The photon selection cuts are indicated by the *dotted lines*

crystal equipped with charged particle veto detector. The narrow photon and the very broad hadron distributions offer the possibility to separate photons and hadrons. A cut of 0.7 $cm \leq D \leq 3.0$ cm results in a hadron rejection of ∼50% with a photon efficiency of ∼75%.

3.3 Calibration and energy resolution

Each detector module is calibrated separately using the pedestal and the signal of minimum ionizing charged particles produced in the collision. In order to account for the longitudinal shower leakage a non-linear extrapolation to higher energies has been used. The shape of this extrapolation is obtained from a GEANT [9] simulation of the energy deposition as a function of the initial energy. For the inner part of the detector array, the energy scale in the high energy region has been determined from data taken with a 10 GeV electron beam. A final tuning of the energy calibration of all detectors has been achieved by an iterative procedure comparing the reconstructed invariant mass peak of the $\pi^\circ \to \gamma\gamma$ signal with that of the accepted π° mass. Using the same method, temperature dependent gain fluctuations of the detectors were also corrected. The energy resolution (RMS) is found to be 3.7% and 5.1% at 170 MeV and 10 GeV, respectively, in good agreement with the expected values from GEANT simulations and earlier measurements [10].

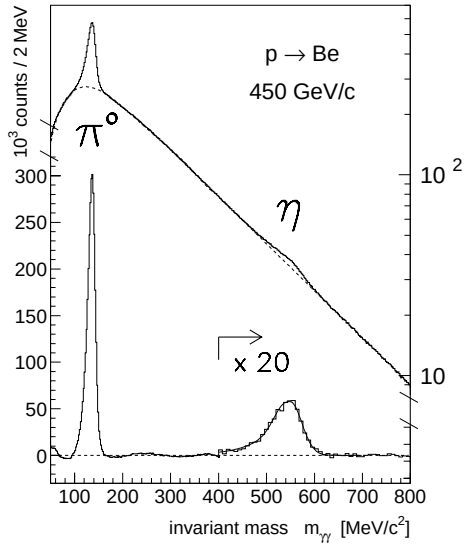

Fig. 3. The $\gamma\gamma$ invariant mass spectrum measured in p-Be collisions. The combinatorial background is indicated by a *dashed line*. In the *lower part* of the figure the background has been subtracted. Note the scale is enlarged by a factor of 20 for masses above 400 MeV/c^2

3.4 Invariant mass analysis

The π° and η mesons are identified via their $\gamma\gamma$ decay and the ω signal via the $\omega \to \pi^\circ\gamma \to \gamma\gamma\gamma$ branch. Figure 3 shows the $\gamma\gamma$ invariant mass spectrum for p-Be. The resonance peaks at the π° and η mass are clearly visible on a large background. The background originates from combinations of photons from different meson decays and is thus unavoidable. It has been fitted with simple analytical functions and subtracted from the data. The result is displayed in the lower part of Fig. 3. The ω signal is extracted from the invariant mass distribution of a π° candidate and a third photon. All photon pairs within $\pm$ 13 MeV/c^2 around the π° mass are considered as π° candidates, but, in calculating the $\pi^0\gamma$ invariant mass the true π° mass is used. In Fig. 4, the background-subtracted spectra for π°, η, and ω are compared to the line shape expected from the known crystal response. Good agreement is achieved. The mass resolution is found to be $\sigma/\mathrm{m} = 5.8\%$ both for π° and η mesons and $\sigma = 7.6\%$ for the ω meson. Due to the variation in opening angles of the $\gamma\gamma$ pair, the mass resolution of the π° signal is dominated by the spatial resolution, whereas the width of the η peak is governed by the energy resolution of the calorimeter. In order to study the transverse mass and rapidity distributions, the invariant mass spectra for different transverse momentum and rapidity bins were analyzed separately. The meson yield extracted for each kinematic bin corresponds to one of the data points shown in Figs. 7 and 8.

3.5 Systematic errors

The systematic errors in photon reconstruction have been estimated by comparing the results of two different photon

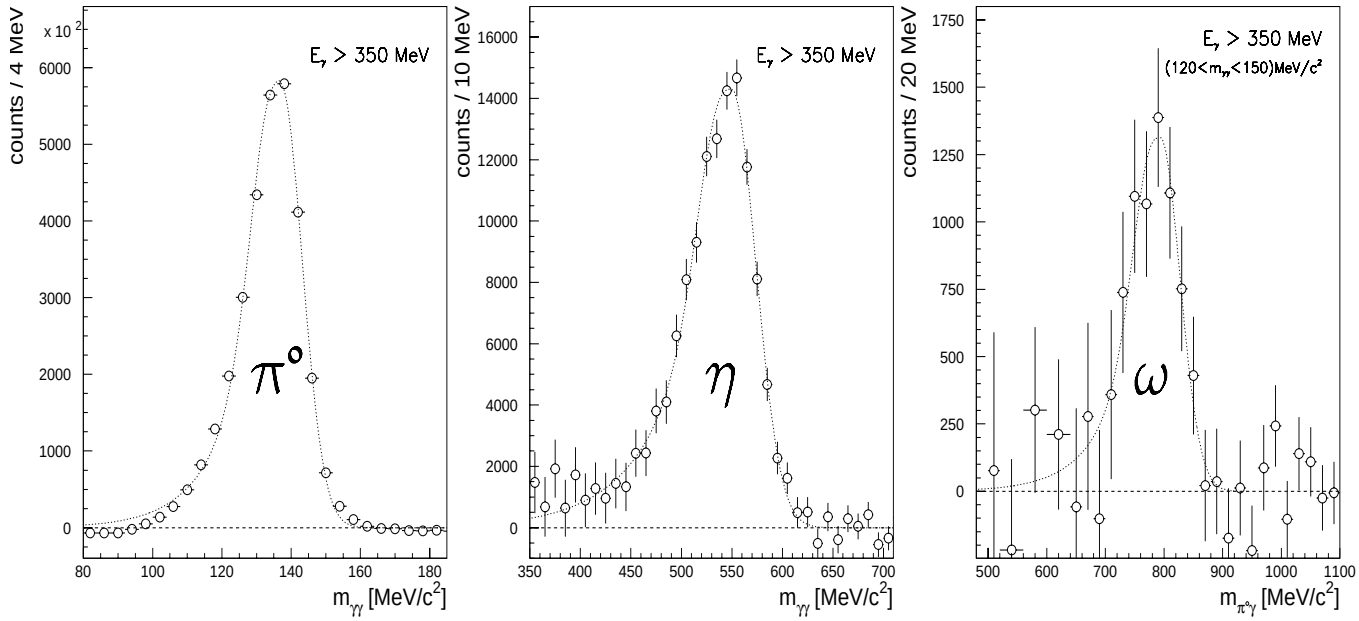

Fig. 4. Background subtracted $\gamma\gamma$ and $\pi^{\circ}\gamma$ invariant mass spectra for p-Be near the π°, η, and ω mass. Also shown is the line shape expected from the detector response. Only photons with energies larger than 350 MeV are used in the analysis

shower reconstruction schemes. One method applies the dispersion cut described in Sect. 3.2, the other one a cut suppressing shower pile-up. The latter cut requires that the maximum energy in any module in the second ring of neighboring detectors is less than 25% of the summed energy in the first ring of neighboring detectors. Both cuts have been optimized through GEANT simulations and agree within 10% when applied to the data, which is taken as the systematic uncertainty in photon shower reconstruction. Because of the high statistics for π° and η mesons, statistical errors are negligible compared to systematic errors, while the opposite holds for the determination of ω meson yields.

4 Simulation of the detector acceptance and efficiency

The detector acceptance and the meson reconstruction efficiency have been determined through Monte-Carlo simulations using GEANT. The different meson species have been simulated according to empirical parameterizations of transverse momentum and rapidity distributions based on M. Bourquin and J.M. Gaillard [1]. The original work has been modified to remove the cusp at $y_{cm} = 0$, which is unphysical and not present in the data, while keeping the link between p_T and y [11].

The simulated events were processed through the same analysis chain as the measured data. The correction for detector acceptance and reconstruction efficiency, including all losses due to cuts in the data analysis, was determined in terms of the ratio of mesons generated within the detector acceptance to those reconstructed in the simulation.

In addition, the reduction of reconstruction efficiency due to overlapping showers caused by high detector occupancy (20% (30%) at a threshold of 10 MeV for p-Be (p-Au)) was estimated using an event overlay method. In order to simulate the effect of the detector occupancy, two reconstructed photon showers (three photons in the case of the ω) were removed from a genuine event and replaced by the hit pattern of the simulated decay photons from a meson. The fraction of simulated mesons that could be reconstructed in this experimental environment determined the occupancy correction. Figures 5 and 6 show the overall efficiencies for the different mesons as a function of rapidity and transverse momentum, respectively. The drop in efficiency at the edge of the rapidity interval $3 < y < 4$ re-

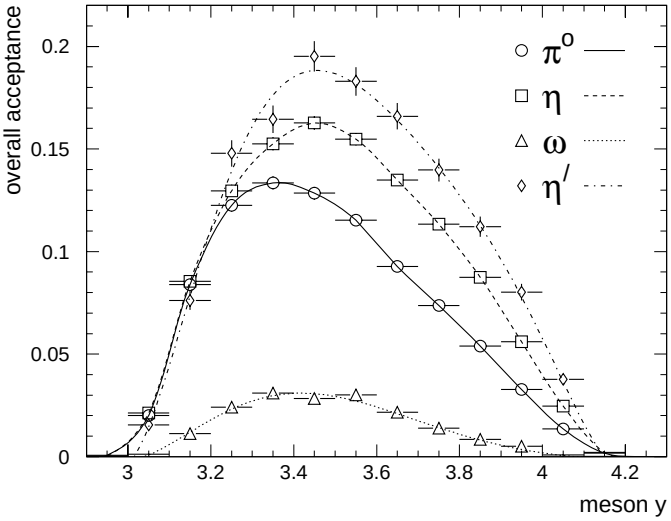

Fig. 5. Combined detector acceptance and reconstruction efficiency as a function of rapidity integrated over all transverse momenta for different mesons

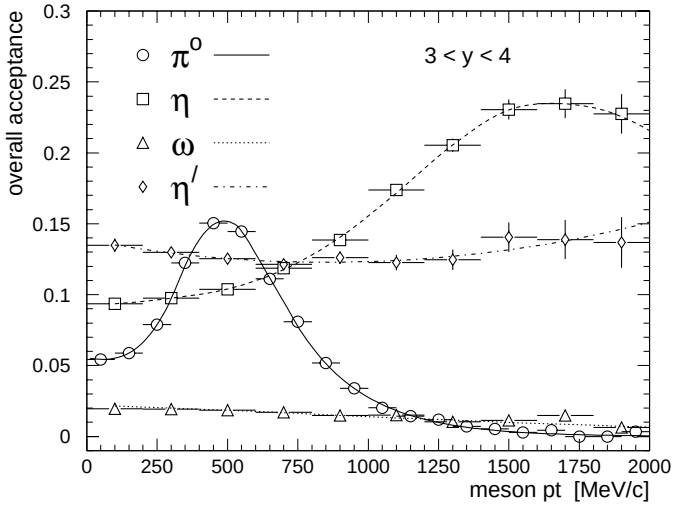

Fig. 6. Combined detector acceptance and reconstruction efficiency as a function of transverse momentum for different mesons in the rapidity interval $3 < y < 4$

flects the loss in geometrical acceptance and can therefore be determined with good precision. With increasing p_T, the geometrical acceptance increases until showers start to overlap. For pions this leads to a peak in the acceptance around a p_T of 500 MeV/c. In principle, the other mesons should show similar behavior, but due to their larger masses, resulting in larger opening angles between the decay photons, the maximum is shifted to much higher transverse momenta.

5 Results

The fully corrected spectra for π°, η, and ω mesons are shown in Fig. 7 as a function of the transverse mass for p-Be and p-Au collisions. The meson production cross section is normalized to the total number of neutral pions produced in the interval $3 < y < 4$. This normalization was chosen to allow a straightforward comparison of the p-Be and p-Au data. The absolute cross sections can be obtained by multiplying the ordinates of Fig. 7 by $\pi^\circ/n_{ch} \cdot \langle\, dN_{ch}/dy \,\rangle \cdot \sigma_{inel}$, where the ratio $\pi^\circ/n_{ch} = 0.47$ can be taken from [12]. For p-Be (p-Au), the average charged particle multiplicity density $\langle\, dN_{ch}/dy \,\rangle$ is 3.0 (4.7) within the calorimeter acceptance [13,14]. The inelastic nuclear cross section is 199 mb (1720 mb) [15]. The data agree to a large extent with a simple m_T-scaling hypothesis. They exhibit the typical exponential-like behaviour, and the spectra are very similar for the two reactions. For both systems, the slopes of the η and ω spectra are nearly identical, while the pion data tend to give the same slope only above $\sim 500\,\mathrm{MeV/c^2}$. At lower transverse mass, it clearly deviates from a simple m_T-scaling hypothesis, as already observed in [16], which points towards a possible contribution from resonance decays to the production of pions with low transverse momentum. The structure in the pion m_T distribution around $\sim 500\,\mathrm{MeV/c^2}$ probably originates from a slight overestimate of the correction for

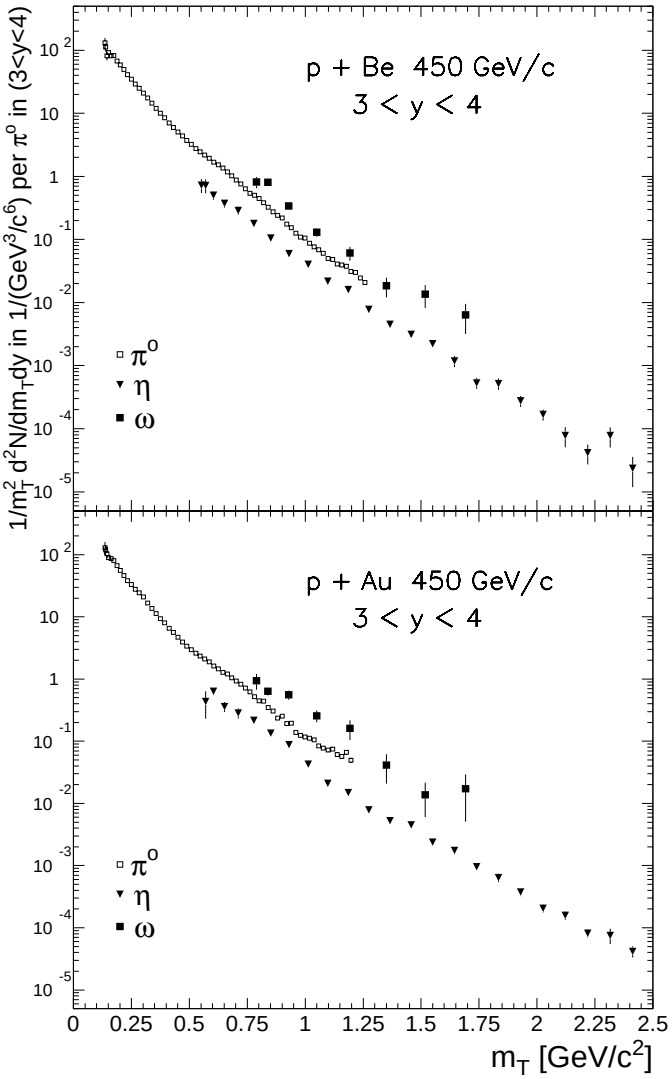

Fig. 7. Transverse mass distributions for the neutral mesons π°, η, and ω produced in p-Be and p-Au collisions. The errors reflect the statistical uncertainties only

efficiency losses due to shower pile-up. The pion data at low m_T – which dominate the integral yield – and the m_T-distributions of the η and ω mesons are not affected by this minor imperfection.

In Fig. 8 we give the rapidity density for the various mesons integrated over m_T. The pion density clearly rises towards the lowest measured rapidities. This is expected for asymmetric collision systems, where the peak of the charged particle density shifts towards target rapidities. For p-Be (p-Au) the maximum charged particle density is reached at rapidity ~ 2.9 (2.4), compared to 3.4 for a p-p collisions at the same $\sqrt{s}$ [14]. It is interesting to note that for the η meson the rapidity density is rather flat between 3 and 3.6, but decreases slightly towards rapidity 4. This could possibly indicate a smaller average shift towards target rapidity for η mesons than for pions.

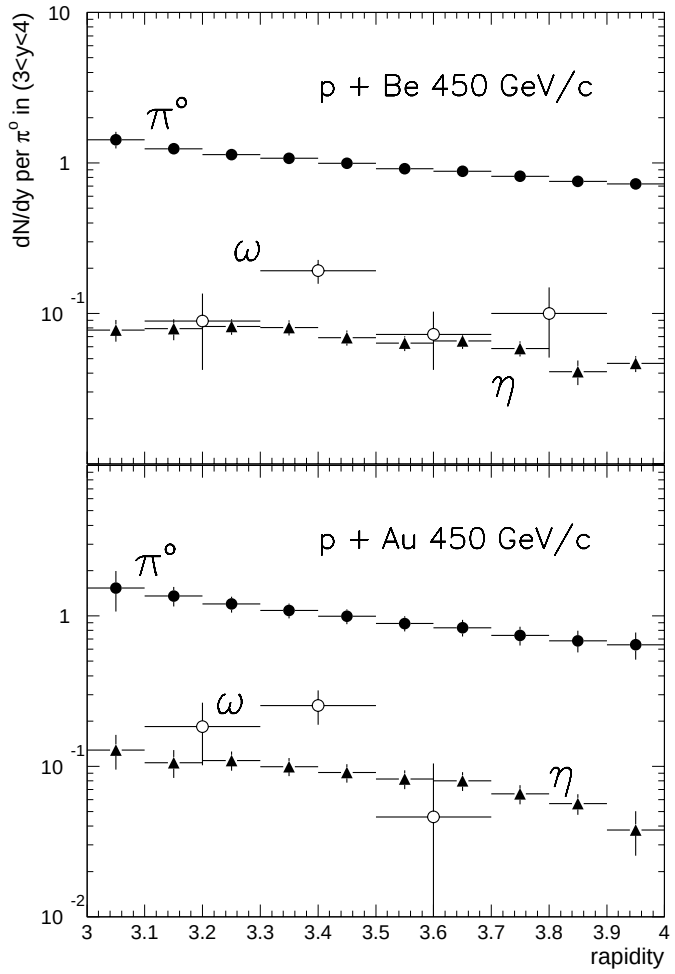

Fig. 8. Rapidity spectra of the measured neutral mesons in the rapidity range $3 < y < 4$. The *upper part* shows the p-Be and *lower part* the p-Au results. Shown are statistical errors combined with the systematic uncertainties due to background subtraction

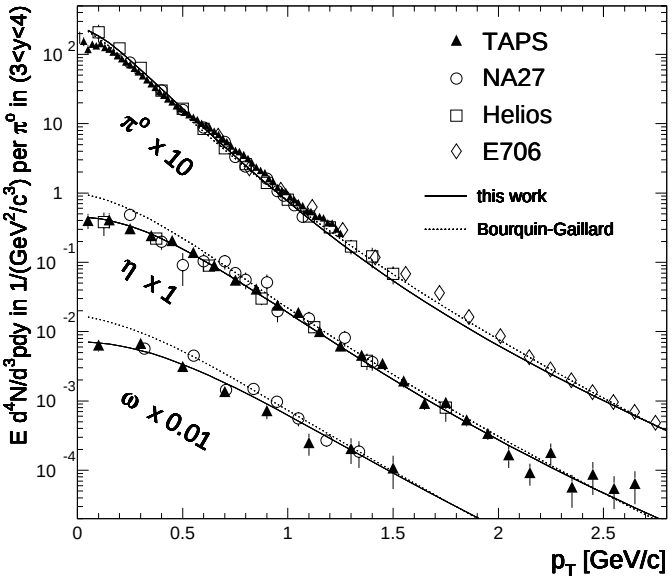

Fig. 9. p-Be invariant cross section as a function of transverse momentum for the different mesons compared to earlier measurements. The *dotted lines* show fits with Bourquin-Gaillard and the *solid lines* with (2). The rapidity intervals covered by the different experiments are qouted in the text

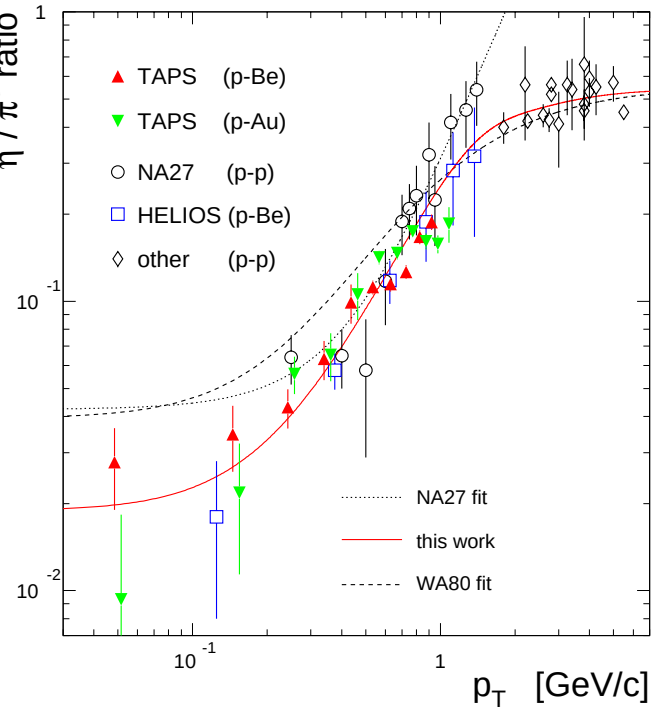

Fig. 10. The η/π° ratio from the data and parameterizations shown Fig. 9. Also shown is the ratio of the fit functions NA27 used to extrapolate the data to low p_T. In addition we have included also our p-Au data

6 Discussion of the results

6.1 Transverse momentum spectra of neutral mesons

In Fig. 9, our data from Fig. 7 are compared to previous measurements. Though all experiments were performed at slightly different conditions, they all measure neutral meson production close to $y_{cm} = 0$, i.e. mid rapidity in the nucleon-nucleon rest frame. Like our experiment, HELIOS [17] investigated p-Be collisions at 450 GeV, but while we cover $-0.4 < y_{cm} < 0.6$, HELIOS had a slightly larger acceptance $-0.2 < y_{cm} < 1.2$. E706 at FERMILAB detected neutral mesons in 500 GeV π-Be interactions in a rapidity interval $-0.7 < y_{cm} < 0.7$ [18]. In the NA27 experiment, neutral mesons were reconstructed for $y_{cm} > 0.5$ in p-p at 400 GeV [12]. We have normalized all π° data relative to our data in order to avoid systematic differences in the absolute normalization of the different data sets. The relative normalization of the different meson species $\pi^\circ : \eta : \omega$ is taken from the original publications. Thus the comparison of different η and ω meson data contains no additional

normalization factor. Note the good agreement of the data from different experiments. Also shown in the figure is the modified Bourquin-Gaillard parameterization [11] for $3 \leq y \leq 4$ and 450 GeV. The calculations are normalized to the data sets at high momenta. They reproduce very well the π^0- data, but significantly overestimate the production rate of η and ω mesons at low transverse momenta. For the new precise η-data the deviation is illustrated more clearly in Fig. 10, where the ratio of η/π° is shown as a function of p_T. This behaviour is easily understood. Most likely the large contribution of resonance decays to the production of low transverse momentum pions accounts for the different behavior of π° compared to η or ω. In the Bourquin-Gaillard, or any other parameterization using m_T as the only parameter distinguishing between the various mesons, an extrapolation to low p_T based on pion data – which was the only low-p_T-data available at the time the BG-parameterization was suggested – cannot be expected to describe heavier mesons. In order to achieve a better description of the low-p_T-region, we use a parameterization with additional parameters (similar to a parameterization suggested earlier by [19]):

$$E\frac{d^3\sigma}{dp^3} = A \cdot \left(\beta_i \cdot \mathrm{e}^{-b_i \cdot m_T} + \alpha_i \cdot \frac{(1-\mathrm{x}_T)^c}{(1+m_T^2)^4} \right) \quad (2)$$

$$\text{with} \qquad \mathrm{x}_T = \frac{2 \cdot m_T}{\sqrt{s}} \qquad \text{and} \qquad i = \pi, \eta, \omega \quad (3)$$

$$\begin{array}{ll} \sqrt{s} = 29.1\,\mathrm{GeV} & c = 7.9 \\ \alpha_\pi = 0.02 & \alpha_\pi = \alpha_\omega = 1.8 \cdot \alpha_\eta \\ \beta_\pi = 1 & \beta_\eta = \beta_\omega = 0.15 \\ b_\pi = 7.5\,\mathrm{GeV}^{-1} & b_\eta = b_\omega = 6.5\,\mathrm{GeV}^{-1} \end{array} \quad (4)$$

In this parameterization, p_T and y are explicitly factorized, which is only valid in a region close to mid rapidity. The first term is a simple exponential in m_T, with different slopes and amplitudes for pions compared to heavier mesons to account for the different low-p_T behavior. The second term is inspired by QCD, and describes the high-p_T part of the spectrum. The parameters were determined by fitting the data in Fig. 9. Due to the large systematic uncertainty, our pion data above 500 MeV/c was not included. The second term is fixed using the E706 data [18] only. The parameter A determines the normalization and is not explicitly quoted. The results shown in Fig. 9 and 10 are in good agreement with all data.

6.2 Relative abundance of neutral mesons

Since an exact determination of the relative neutral meson abundances is of utmost importance in order to determine the dilepton yield from hadron decays – the primary goal of this experiment – we compare in this section our data to results of previous experiments in a more quantitative way. Throughout this section we compare production cross sections integrated over p_T in the rapidity interval $3.1 < y < 3.7$. We have restricted the acceptance for our data to avoid large corrections at the boundaries. Wherever necessary, we have extrapolated the data of other experiments to our rapidity region, taking into account the measured reduction of the width of the rapidity distribution with the meson mass [12]. We have always used the originally published extrapolation to low p_T. In addition, we focus on ratios of cross sections so as to be less sensitive to systematic errors in absolute normalization of different experiments. The results of our compilation are summarized in Table 1. Statistical and systematic errors have been added quadratically.

Table 1. Comparison of relative cross sections integrated over p_T in the rapidity range $3.1 < y < 3.7$. Data not measured in this rapidity range have been extrapolated to this region with the modified Bourquin-Gaillard distribution [11]. The results of the HELIOS measurement can be found in [17], the NA27 data are from [12].(* Estimated, assuming to be the same as $\eta/2\omega$.)

Experiment	η/π° **ratio**	ω/π° **ratio** (ρ/π° **ratio**)	$\eta/(\rho+\omega)$ **ratio**
TAPS p-Be	6.9±0.5 %	10.2±2.0 %	34±8 %*
TAPS p-Au	8.8±1.1 %	12.0±3.4 %	37±11 %
HELIOS p-Be	6.9±0.8 %	-	43±5 %
NA27 p-p	9.3±0.8 %	13.3±1.2 % (14.8±1.1 %)	34±4 %

The η/π° ratio found by HELIOS, which has also directly measured π° and η at low p_T, agrees with our value within the errors. In contrast, extrapolating the NA27 data [12] to our rapidity acceptance we find a ratio approximately 25% larger than our value. The difference is shown in Fig. 11 as a function of rapidity. NA27 has measured η and π° only above $y_{cm} > 0.5$, but clearly the discrepancy does not arise from the extrapolation to $y_{cm} = 0$. Careful inspection of Fig. 9 shows that the NA27 η-spectrum is higher compared to ours or to the HELIOS spectrum for $p_T \leq 1$ GeV/c. As a consequence, these higher points lead to the fit used by NA27, which significantly deviates from our data below 400 MeV/c, as shown in Fig. 10. An earlier measurement by Kass et al. [20], which gave an upper limit for the η/π^0 ratio of $\leq 6.4\%$, is compatible with our result.

For the ω/π°-ratio, also given in Table 1, we again observe a slightly lower value compared to the NA27 data. The NA27 value for the ω/π°-ratio is well in line with their ρ/π°-ratio, as expected, since ρ and ω have similar mass and quark content. A compilation of ρ-data from other experiments supports the large value of ρ/π° [21]. However, common to all these estimates is the extrapolation of the data to low p_T, based on p_T-distributions that are steeper than suggested by our data. We have therefore determined the ratio η/ω, for which the uncertainty of the extrapolation should cancel. Since a value for $\eta/(\rho+\omega)$ is available also from HELIOS [22], we have quoted this ratio in Table 1, using $\eta/2\omega$ for our measurements. For this ratio, a good agreement is achieved between our value and the value derived from the NA27 data. The HELIOS value is slightly higher, however, this measurement is determined from muon pair data, and involves several extrapolations,

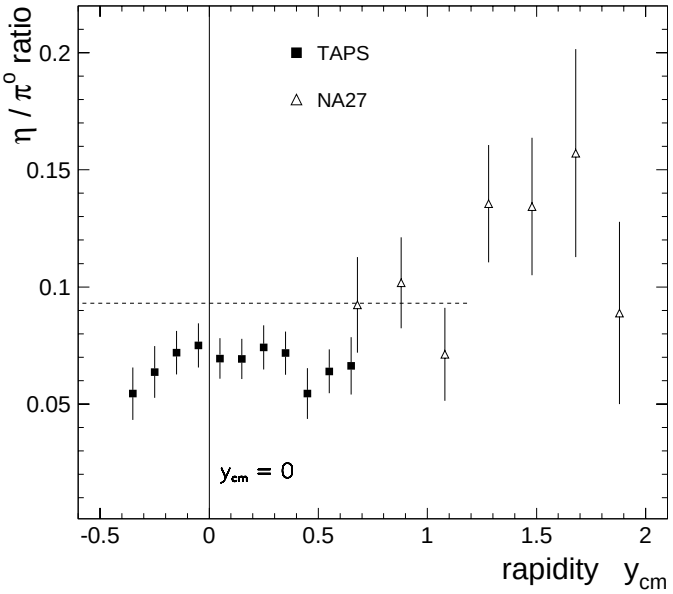

Fig. 11. Ratio of the cross sections after integration over p_T for η/π° as a function of rapidity, measured by TAPS (this work) and by NA27 [12]. The *horizontal line* corresponds to the η/π^0 -ratio deduced from the NA27 data

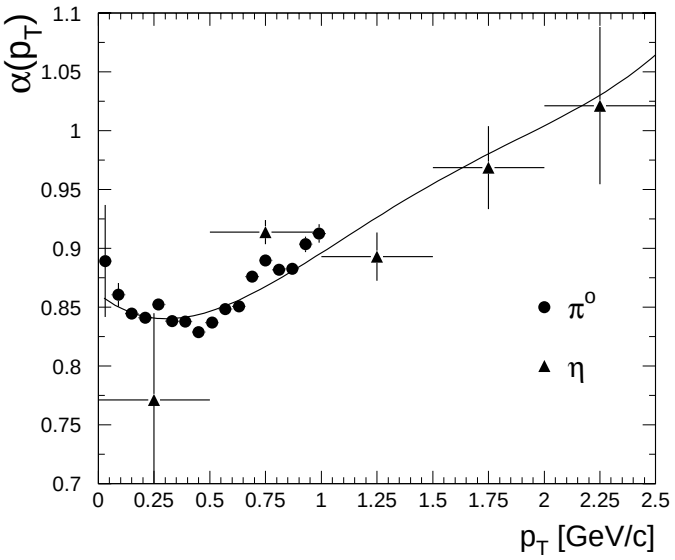

Fig. 12. Power α of the A dependence as a function of transverse momentum for the different mesons ($\alpha = ln\left(\frac{\sigma_{Au}}{\sigma_{Be}}\right) / ln\left(\frac{A_{Au}}{A_{Be}}\right)$). The absolute normalization for our p-Be and p-Au data was obtained as outlined in Sect. 5

e.g. correcting for the ρ/ω interference in the $\mu^+\mu^-$ decay channel.

We have also made an attempt to reconstruct $\eta' \to \gamma\gamma$ decays in our p-Be data, but no reliable signal could be derived. We have estimated that, at a confidence level of 95%, our data limits the η'/η-ratio to less than 0.2. This value is somewhat lower than the one derived from an extrapolation of high-p_T η and η' data, which yields $\eta'/\eta = 0.3$ [23].

6.3 A dependence of neutral meson production

Table 1 compares the ratios of neutral meson production cross sections we have measured in p-Be collisions with those extracted from the p-Au data. Both η/π° and ω/π° ratios are slightly larger for p-Au, though the effect is not significant. A small increase might be expected if the rapidity shift towards target rapidity in asymmetric collision systems is smaller for heavier mass mesons than for pions. Some indication for a smaller shift of the η compared to the π° has already been observed in Fig. 8. But, like the difference in the particle ratios, the evidence is not significant.

Neglecting the small difference in the acceptance due to the different rapidity shifts in p-Be and p-Au, we have analyzed the p_T-spectra in terms of $\sigma_{pA} = A^\alpha \sigma_{pp}$ using a p_T-dependent exponent $\alpha(p_T)$. Such parameterizations of the A dependence have been used frequently ever since the discovery of the so-called anomalous nuclear enhancement of pions and kaons in the 70's [16,24]. In Fig. 12 $\alpha(p_T)$ is shown for π° and η. Also shown is a fit to previously measured charged pion data [16,18,24–26]. Our pion data is in very good agreement with this fit and in particular corroborates the slight increase of α observed for very low p_T charged pions [25]. The η meson reveals a similar A dependence as the pions. For the ω meson our data are not conclusive.

7 Conclusions

We have measured the production of neutral mesons π°, η, and ω in p-Be and p-Au collisions at 450 GeV in a narrow interval around mid-rapidity. The π° p_T-distribution is well in line with previous measurements. Our precise data on η-production at low p_T, however, reveals a lower cross section than expected from extrapolating data at higher p_T, in agreement with recent HELIOS results. A similar observation is made for the ω meson, though with somewhat less accuracy. From a comparison of all available data we conclude that both η- and ω-production may have previously been overestimated by 25-30 % at low p_T. Within the accuracy of our measurement, we observe no change in the relative abundance of π°, η, and ω comparing p-Be and p-Au data. For the η the A dependence as a function of p_T is very similar to the well known "Cronin-effect" for pions.

Based on these new data, we have estimated the contribution of hadron decays to the production of low mass e^+e^--pairs in p-Be and p-Au collisions, and demonstrated in [5] that the systematic uncertainty is thereby greatly reduced compared to previous studies.

Acknowledgements. We would like to express our sincere gratitude to the specialists of the CERN SPS. This work was supported in part by Gesellschaft für Schwerionenforschung (GSI) and by Deutsches Bundesministerium für Bildung, Wissenschaft, Forschung und Technologie (BMBF) under the con-

tracts No. 06 HD 525 I and No. 06 GI 475 I (3), by the Israel Science Foundation, by the German-Israeli Foundation for Scientific Research and Development, and by a research grant from the Clarisse and Cornelius Gustav Memorial Fund.

References

1. M. Bourquin and J.M. Gaillard, Nucl. Phys. B **114**, 334 (1976)
2. G.B. Bondarenko et al., Phys. Lett. B **64**, 365 (1976); K.J. Anderson et al., Phys. Rev. Lett. **37**, 799 (1976); J. Ballam et al., Phys. Rev. Lett. **41**, 1207 (1978); D. Blockus et al., Nucl. Phys. B **201**, 205 (1982); M.R. Adams et al., Phys. Rev. D **27**, 1977 (1983); T. Åkesson et al., Phys. Lett. B **192**, 463 (1987)
3. T. Åkesson et al., Z. Phys. C **68**, 47 (1995)
4. CERN/SPSC 92-48 Addendum II to Proposal SPSC/P237
5. G. Agakichiev et al., this issue of Z. Phys. C
6. R. Novotny, IEEE Trans. Nucl. Sci. **38**, 379 (1991)
7. R. Baur et al., Nucl. Instr. and Meth. A **343**, 87 (1994)
8. T. F. Günzel et al., Nucl. Instr. and Meth. A **316**, 259 (1994)
9. R. Brun et al., GEANT3, CERN/DD/cc/84-1
10. A.R. Gabler et al., Nucl. Instr. and Meth. A **346**, 168 (1994)
11. G. Tel-Zur, PhD Thesis, Weizmann Institute of Science, Rehovot, Israel, 1996
12. M. Aguilar-Benitez et al., Z. Phys. C **50**, 405 (1991)
13. Y. Lee, Diploma Thesis, Universität Heidelberg, 1994
14. W. Busza and R. Ledoux, Ann. Rev. Nucl. Part. Sci. **38**, 119 (1988)
15. Review of Particle Properties, Phys. Rev. D **45**, 1 (1992)
16. D. Chaney et al., PRD **19**, 3210 (1979)
17. V. Tikhomirov, HADRON 95, Proceedings of the 6th International Conference on Hadron Spectroscopy (World Scientific Publishing, 1995)
18. T. Ferbel, Proc. of the XXXIst Rencontres de Moriond, Les Arcs, France (1996) and references therein.
19. B. Alper et al., Nucl. Phys. B **100**, 237 (1975)
20. R.D. Kass et al., Phys. Rev. D **20**, 605 (1979)
21. M.G. Albrow et al., Nucl. Phys. B **155**, 39 (1979)
22. R. Veenhof, Doctoral Thesis, University of Amsterdam, 1993
23. M. Diakonou et al., Phys. Lett. B **89**, 432 (1980)
24. D. Antreasyan et al., Phys. Rev. D **19**, 764 (1979)
25. D.A. Garbutt et al., Phys. Lett. B **67**, 355 (1977)
26. H. Frisch et al., Phys. Rev. D **27**, 1001 (1983)